Molecular Vision 2020; 26:277-290 <http://www.molvis.org/molvis/v26/277>
Received 24 July 2019 | Accepted 9 April 2020 | Published 11 April 2020

Proinflammatory cytokines trigger biochemical and neurochemical changes in mouse retinal explants exposed to hyperglycemic conditions

Gaganashree Shivashankar,[1] Julie C. Lim,[2] Monica L. Acosta[1]

[1]School of Optometry and Vision Science and New Zealand National Eye Centre, University of Auckland, Auckland, New Zealand; [2]Department of Physiology, School of Medical and Health Sciences and New Zealand National Eye Centre, University of Auckland, Auckland, New Zealand

Purpose: Diabetic retinopathy (DR) is one of the most frequent complications of diabetes affecting the retina and eventually causing vision impairment. Emerging evidence suggests that inflammation plays a vital role in DR progression. In this study, we evaluated the early biochemical and neurochemical changes in mouse retinal explants to understand the contribution of proinflammatory cytokines to disease progression.

Methods: DR was modeled in vitro by incubating mouse retinal explants in a physiological buffer supplemented with high glucose and the proinflammatory cytokines TNF-α and IL-1β. Key metabolites of retinal energy metabolism, including glucose, lactate, ATP, glutamate, glutamine, and enzymes supporting retinal ATP levels were assessed 40 min after the application of high glucose and proinflammatory cytokines. As retinal energy metabolism is tightly coupled to retinal neurochemistry, we also determined the short-term effect on the amino acid distribution of glutamate, gamma aminobutyric acid (GABA), glutamine, and glycine.

Results: The results indicated that the combined application of high glucose and proinflammatory cytokines increased retinal glucose, lactate, and ATP levels, and decreased retinal glutamate, without affecting glutamine levels or the enzymes supporting ATP levels. Moreover, we observed a statistically significant increase in ATP and glutamate release. Correspondingly, statistically significant alterations in amino acid distribution were observed in retinal explants coexposed to high glucose and proinflammatory cytokines.

Conclusions: These data suggest that short-term exposure to proinflammatory cytokines contributes to the early biochemical and neurochemical changes caused by hyperglycemia, by affecting retinal energy metabolism and amino acid distribution. These data are consistent with the idea that early intervention to prevent inflammation-triggered loss of metabolic homeostasis in patients with diabetes is necessary to prevent DR progression.

Diabetic retinopathy (DR) is one of the most frequent microvascular complications affecting the retina in patients with diabetes and a common cause of vision impairment. Although the pathogenesis of DR is multifactorial, hyperglycemia alone has been regarded as the primary pathological factor inducing retina vascular changes and retinal injury in patients with DR [1,2]. However, a growing body of evidence has shown that in addition to high glucose levels, proinflammatory cytokines elicit an inflammatory response in the diabetic retina [3-7], which precedes vascular impairment [8]. Most studies have explained DR pathology when inflammation is already present in the retina, but there are limited studies showing how high glucose and proinflammatory cytokines affect early retinal metabolism [6,7]. Thus, the aim of this study was to determine the early retinal biochemical and neurochemical changes when hyperglycemia occurs in an inflammatory environment.

Under normal physiological conditions, the retina has high and fluctuating energy demands, which are largely dependent on glucose, as the metabolic substrate to generate ATP via glycolysis and oxidative phosphorylation [9]. Furthermore, a high rate of lactate production via aerobic glycolysis occurs in the retina [10], which is further metabolized to pyruvate by lactate dehydrogenase (LDH) to support the high ATP demand [11]. In addition to LDH, the other commonly studied metabolic enzyme in the retina is creatine kinase (CK). CK supports and maintains the high energy demand in photoreceptors by catalyzing the transportation of high-energy phosphate groups [12]. Although LDH and CK have been widely investigated to determine the metabolic status of the retina during retinal pathology [13-15], their activity in response to high glucose with concomitant activation of an inflammatory process is unknown.

In addition to glucose, the high energy demand of the retina is supported by anaplerotic reactions, which replenish

Correspondence to: Monica L. Acosta, School of Optometry and Vision Science, University of Auckland, 85 Park Road, Auckland-1023, New Zealand. Phone: +64 9 3737599 ext. 86069; email: m.acosta@auckland.ac.nz

the tricarboxylic acid (TCA) cycle intermediates at the expense of neurotransmitters [16]. Glutamate, the most prevalent excitatory neurotransmitter in the retina, is also a critical anaplerotic substrate that is affected during periods of metabolic stress [17,18], including in DR [19]. Within the retinal neurons, glutamate is synthesized from its precursor metabolite, glutamine, and is consumed for several purposes, including neurotransmission, ATP production via the TCA cycle, and synthesis of inhibitory neurotransmitter gamma-aminobutyric acid (GABA) [20-22]. Aspartate aminotransferase (AST) and glutamate dehydrogenase (GDH) are critical anaplerotic enzymes that regulate metabolic glutamate to replenish the TCA cycle substrates and have been associated with retinal metabolic changes [14,23]. The contribution of these enzymes in regulating retina glutamate levels during DR has not been studied, but it is known that there is substantial neurotransmitter redistribution as a function of DR progression [24,25]. Thus, in this study we evaluated the early effect of high glucose and proinflammatory cytokines on retinal energy metabolism and amino acid distribution.

METHODS

Animals: All animal procedures were approved by the University of Auckland Animal Ethics Committee (AEC 1462 and AEC 2018) and were conducted in accordance with the Association for Research in Vision and Ophthalmology (ARVO) statement on the use of animals in research. Six- to seven-week-old female C57BL/6J mice obtained from Jackson Laboratory (Bar Harbour, ME), inbred and housed at the Vernon Jansen Unit, University of Auckland, were used in this study. The mice were euthanized by cervical dislocation, and the eyes were enucleated immediately to avoid the onset of ischemia. The anterior segment was discarded, and the posterior eye cup was gently teased to detach the retina from the RPE and the choroid/sclera. Each retina was transferred to an incubation chamber containing physiological buffer.

In vitro retinal incubations: An in-house retina incubation system adapted and modified according to previous studies [14,26] was used for short-term retinal incubations. Briefly, an air-tightened incubation chamber was supplied with carbogen gas (95% O_2 and 5% CO_2) delivered via a thin capillary tube. The capillary tube was connected to a pressurized gas tank, which supplied the desired gas mixture to the incubation chamber. The retinal samples were incubated simultaneously at 37 °C for 40 min in the physiological buffer prepared with 125 mM NaCl, 2.5 mM KCl, 26 mM $NaHCO_3$, 1.25 mM NaH_2PO_4, 10 mM D-glucose, 2 mM $CaCl_2$ and 1 mM $MgCl_2$. The physiological buffer was bubbled with carbogen gas (95% O_2 and 5% CO_2) for at least 1 h at 37 °C before the incubation period, and throughout the incubation period [14,27]. Hyperglycemia was modeled in vitro by supplementing the physiological buffer containing 10 mM glucose with an additional 20 mM of D-glucose. To rule out a possible osmotic effect by high glucose, incubations were also conducted in the physiological buffer supplemented with 20 mM D-mannitol. As no statistically significant changes in biochemical and neurochemical assays were observed using D-mannitol, we concluded that the metabolic changes observed in the study were not related to osmolarity induced changes (Appendix 1).

Hyperglycemia in the presence of proinflammatory cytokines was modeled in vitro by supplementing the physiological buffer with 10 ng/ml TNF-α (#RMTNFAI, Thermo Fisher Scientific, Waltham, MA), 10 ng/ml IL-1β (#RMIL1BI; Thermo Fisher Scientific), and 20 mM of D-glucose. The physiological buffer supplemented with 10 ng/ml TNF-α and 10 ng/ml IL-1β was used as a proinflammatory cytokine-only control. As a positive control of metabolic changes in the mouse retinal explants during in vitro short-term incubation, the retina was incubated in an anoxic buffer created by bubbling the physiological buffer with 95% N_2 and 5% CO_2 before and during the incubation [14]. The details of the incubation conditions are summarized in Table 1.

Following the 40-min incubation, the retina and the incubation buffer were collected separately. The retina was homogenized in ice-cold 0.9% NaCl, in a glass-Teflon homogenizer, and centrifuged at 5000 ×*g* for 10 min at 4 °C. The retinal supernatant was collected. Post-incubation, the buffer was centrifuged using the same centrifugation parameters to remove any cellular debris. Henceforth, the terms "retina" and "incubation buffer" mean the post-incubation homogenized retinal supernatant and the post-incubation buffer, respectively.

Protein quantification: The protein concentration of the retina was determined using the Direct Detect® Infrared Spectrometer (Merck Millipore, Darmstadt, Germany), which measures amide bonds in the protein chain. The spectrophotometer performs fast infrared analysis of the aqueous samples presented in a dried format on a hydrophilic polytetrafluoroethylene (PTFE) membrane [28]. To determine the protein concentration, 2 µl of the retinal sample was spotted onto the PTFE membrane on an assay card along with a buffer-only sample, as a reference blank. Protein concentration is expressed in milligrams per milliliter.

Glucose, lactate, and glutamate-glutamine assays: The levels of retinal glucose (Glucose-Glo™ Assay, #J6021; Promega, Madison, WI), lactate (Lactate-Glo™ Assay, #J5021; Promega), glutamate-glutamine (Glutamine/Glutamate-Glo™

Assay, #J8021; Promega), and their release into the incubation buffer were determined according to the manufacturer's protocol. Briefly, the retina or the incubation buffer was mixed with an inactivation solution (0.6 N HCl) and a neutralization solution (1 M Tris base) in a 8:1:1 ratio to halt cellular metabolism, inhibit endogenous enzyme activity, and destroy any endogenous reduced NADH dinucleotides and allow reading of the desired enzyme.

To estimate the glutamate-glutamine levels in the retina and incubation buffer, samples were incubated with and without glutaminase for 40 min, following which, the glutamate detection reagent was added in a 1:1 ratio and incubated for a further 60 min. This reaction couples glutamate oxidation to NADH production and the subsequent conversion of pro-luciferin to luciferin, which is then used by luciferase. The luminescence signal generated was recorded using the EnSpire® Multimode Plate Reader (Perkin Elmer, Waltham, MA). The glucose and lactate levels were determined using a similar protocol, where the retinal supernatant and the incubation buffer were treated separately with their respective detection reagents for 60 min at room temperature and the luminescence signal recorded. The glucose, lactate, glutamate, and glutamine levels are reported as nanomoles per milligram of protein.

ATP assay: The level of ATP in the retina and the incubation buffer was determined using the Adenosine 5′-Triphosphate (ATP) Bioluminescent Assay Kit (#FLAA, Sigma-Aldrich, St Louis, MO) according to the manufacturer's protocol. Briefly, fresh ATP assay mix working solution was prepared by diluting the ATP assay mix stock solution (containing luciferase, luciferin, $MgSO_4$, DTT, EDTA, bovine serum albumin (BSA), and tricine buffer salts) with ATP assay mix dilution buffer (containing $MgSO_4$, DTT, EDTA, BSA, and tricine buffer salts) in a 1:25 ratio. To the ATP assay mix working solution, the retinal supernatant or the incubation buffer was added, and the luminescence signal generated by the oxidation of D-luciferin was recorded immediately using the EnSpire® Multimode Plate Reader (Perkin Elmer). The ATP levels are reported as picomoles per milligram of protein.

Enzyme activities in the retina: CK and AST activities were determined using the CK-NAC Reagent (# TR14010, Thermo Fisher Scientific) and Infinity™ AST (GOT) Liquid Stable Reagent (# TR70121, Thermo Fisher Scientific), respectively, according to the manufacturer's protocol. Briefly, retinal supernatant was added to CK-NAC Reagent in a 1:20 ratio. The reagent contained 100 mM bis-Tris Buffer, 31.5 mM creatine phosphate, 5.3 mM AMP, 2.2 mM NADP, 2.1 mM EDTA, 10.3 µM AP5A, 10.5 mM Mg^{2+}, 2.5 mM ADP, 21 mM D-glucose, 21 mM N-acetyl-l-cysteine, >3000 U/l hexokinase (yeast), and >2000 U/l G-6-PDH (*Leuconostoc*). The rate of the NADH absorbance change was measured at 340 nm using the EnSpire® Multimode Plate Reader (Perkin Elmer). Similarly, the retinal supernatant was added to the AST reagent in a 1:10 ratio. The reagent contained 13 mM 2-oxoglutarate, 220 mM L-aspartate, >100 U/l MDH (microbial), >1500 U/l LDH (microbial), >0.12 mM NADH, 88 mM Tris buffer, and 5 mM EDTA. The rate of change in the absorbance of NADH

Table 1. In vitro incubation conditions used in this study.

Incubation condition	Incubation buffer	Supplement to incubation buffer	Gas mixture	Phenotype
Control	Normal physiological buffer	-	95% O_2 & 5% CO_2	Normal
High glucose	Normal physiological buffer	20 mM Glucose	95% O_2 & 5% CO_2	Hyperglycemia
High glucose + proinflammatory cytokines	Normal physiological buffer	20 mM Glucose, 10 ng/ml IL-1β, 10 ng/ml TNF- α	95% O_2 & 5% CO_2	Hyperglycemia with inflammation
D- Mannitol	Normal physiological buffer	20 mM D- Mannitol	95% O_2 & 5% CO_2	Osmotic control
Proinflammatory cytokines	Normal physiological buffer	10 ng/ml IL-1β, 10 ng/ml TNF- α	95% O_2 & 5% CO_2	Cytokines control
Anoxia	Normal physiological buffer	-	95% N_2 & 5% CO_2	Cellular damage control

The normal physiological buffer was prepared with 125 mM NaCl, 2.5 mM KCl, 26 mM $NaHCO_3$, 1.25 mM NaH_2PO_4, 10 mM D-Glucose, 2 mM $CaCl_2$ and 1 mM $MgCl_2$. The physiological buffer was bubbled with carbogen gas (95% O_2 and 5% CO_2) for at least 1 h at 37 °C before incubation, and throughout the incubation. The physiological buffer was supplemented with D-glucose, proinflammatory cytokines, D-mannitol and bubbled with 95% N_2 & 5% CO_2 to model various metabolic phenotype.

was measured at 340 nm. The specific enzyme activities are expressed as micromoles per minute per milligram of protein.

LDH activity was determined in a kinetic manner using the Cytotoxicity Detection Kit (# 11644793001; Roche, Basel, Switzerland) with modification. Because the kit does not measure LDH activity directly, we determined the rate of change in the absorbance (the rate of formazan product formation) every 3 min, for a total of 15 min at 490 nm. The LDH activity was determined based on the standard calculations of enzyme activity, using 27.5 as the millimolar absorption coefficient of formazan at 490 nm [29]. LDH activity is expressed as micromoles per minute per milligram of protein.

GDH activity was determined using the Glutamate Dehydrogenase Kit (# ab102527; Abcam, Cambridge, UK) according to the manufacturer's protocol. Briefly, the retina was homogenized in GDH assay buffer and centrifuged at 13,000 ×*g* for 10 min to remove any cellular debris. The retinal supernatant was added to the reaction mix containing GDH assay buffer, GDH developer, and 2 M glutamate and incubated for 30 min. Absorbance was measured at 3 min and 30 min at 450 nm. GDH activity is expressed as nanomoles per minute per milligram of protein.

Silver intensified immunogold immunohistochemistry: Following the in vitro incubations, the retina samples were immediately fixed in a solution of 2.5% glutaraldehyde and 1% paraformaldehyde in phosphate buffer, pH 7.4 for 60 min. Following fixation, the samples were processed and embedded in eponate resin according to standard protocols [30]. Subsequent to embedding, the retina was sectioned at 500 nm thickness using a Leica Ultracut UCT ultra microtome (Leica Microsystems, Wetzlar, Germany). The detailed method for post-embedding silver intensified immunohistochemistry has been previously described [30,31]. Briefly, single sections were collected on teflon coated slides (Celline, Newfield, NJ). The retinal sections were deplasticized in 1:5 solution of sodium ethoxide: ethanol and washed in graded series of ethanol and a final wash in phosphate buffer. The slides were then placed in 1% sodium borohydride for 30 min, following which they were washed in phosphate buffer and quickly dried before applying 3% goat serum in phosphate buffer saline to block non-specific binding sites for 1 h. The primary antibodies were applied overnight followed by nanogold-conjugated secondary antibody incubation for 3 h. The slides were then washed in phosphate buffer and fixed with 1% glutaraldehyde in phosphate buffer for 10 min. The nano-gold labeling was visualized by silver intensification.

The primary antibodies used were rabbit polyclonal anti-glutamate (1:250; ab9440, Abcam), anti-glutamine (1:250; ab9445, Abcam) anti-GABA (1:50; ab9446, Abcam), and anti-glycine (1:25; ab9442, Abcam). A 1.4 nm Nanogold® conjugated, immunoglobulin (IgG), goat anti-rabbit secondary antibody (GαR-gold; 1:100, #2003; Nanoprobes, New York, NY) was used. All retina sections were processed under identical immunolabeling and silver intensification procedures, which allowed comparison of the retinal neurotransmitter levels within and across incubation groups.

Quantification of amino acid distribution within the retina: A Leica DMRA2 upright microscope (Leica Microsystems) was used to visualize the silver intensified immunolabeling, and grayscale images were captured using a Leica DFC495 camera (Leica Microsystems) mounted on the microscope under fixed parameters of exposure time, gamma, brightness, and contrast using Leica Application Suite Version 4.8.0. The labeling was quantified using Image J software (National Institutes of Health-NIH). A histogram tool was used to quantify the neurotransmitter labeling in the images, where the pixel values ranged from 0 to 255. To compare the neurotransmitter labeling across the retinal cells, a fixed circular area equivalent to 100 pixels was drawn in selected areas and the mean pixel value recorded. Data were collected from different retinal layers, and the mean pixel value outside the retina was used as the background signal, which was subtracted from the values obtained from the retinal layers. Pixel values were obtained from identified retinal areas corresponding to the ganglion cell layer, Müller cell endfeet, inner plexiform layer, amacrine cells, bipolar cells, Müller cell soma, outer plexiform layer, outer nuclear layer, and photoreceptor inner and outer segments. The results were plotted as a relative change in immunoreactivity compared to the control retina (expressed in arbitrary units).

Statistical analysis: For the biochemical assays (n = 6–8 per condition), each value represents the mean value or activity normalized to the retina protein concentration and is presented as mean ± standard error of the mean. Statistical comparison between the incubation conditions was performed using one-way ANOVA, and the post-hoc Dunnett's multiple comparison test was used to compare each data point to control data points. For immunogold labeling (n = 4 per condition), each value represents the mean difference in immunoreactivity relative to the control condition and is presented as a percentage change ± standard error of the mean. The statistical significance was determined using ANOVA and the post-hoc Dunnett's multiple comparison test. All statistical analysis were performed using GraphPad Prism 8, and a p value of less than 0.05 was considered statistically significant.

RESULTS

Short-term exposure to high glucose and proinflammatory cytokines does not induce cytotoxicity: To ensure the metabolic changes in mouse retinal explants were in response to the experimental incubation conditions, and not due to experimental cytotoxicity, we evaluated the LDH released into the medium 40 min after in vitro incubation (Figure 1). Although there was a statistically significant increase in LDH activity in anoxic conditions ($p = 1 \times 10^{e-6}$) compared to the control condition, there were no changes in the LDH release in the retinas incubated in high glucose and proinflammatory cytokines alone and in combination. This result indicated that the experimental incubation conditions in high glucose and proinflammatory cytokines alone and in combination were not as damaging to the retina as the lack of oxygen.

Coapplication of high glucose and proinflammatory cytokines affects energy metabolism: We evaluated the effect of high glucose and proinflammatory cytokines alone and in combination on the retinal glucose (Figure 2A), lactate (Figure 2B), and ATP (Figure 2C) levels in the mouse retinal explants. Coapplication of high glucose and proinflammatory cytokines resulted in a statistically significant 1.6-fold increase in glucose (p = 0.039), a 1.7-fold increase in lactate (p = 0.005), and a 1.4-fold increase in ATP (p = 0.016) levels compared to the control retinas. Moreover, there was a statistically significant 3.4-fold increase in ATP release (p = 0.002) compared to the control without affecting the lactate release.

CK, LDH, AST, and GDH activities in the retina were unaffected: To determine whether additional ATP-related pathways in the retina were influencing the high ATP levels, we evaluated the specific activities of the retinal CK, LDH, and anaplerotic enzymes AST and GDH. However, high glucose and proinflammatory cytokines alone and in combination did not affect the retinal CK (Figure 3A), LDH (Figure 3B), AST (Figure 3C), and GDH (Figure 3D) activities compared to the control retinas.

Coapplication of high glucose and proinflammatory cytokines affects glutamate metabolism: We evaluated the effect of high glucose and proinflammatory cytokines alone and in combination on retinal glutamate (Figure 4A) and its precursor, glutamine (Figure 4B). There was a statistically significant 1.4-fold decrease in the glutamate levels in high glucose alone (p = 0.032) and in combination with proinflammatory cytokines (p = 0.043) compared to the control retinas. However, no changes were observed in the retinal glutamine levels in any of the experimental incubations compared with the control retinas. The reduction in the retinal glutamate level was accompanied by a statistically significant 1.5-fold increase in the glutamate release during coapplication of high glucose and proinflammatory cytokines (p = 0.008) compared to the control retinas. The glutamine release was not affected.

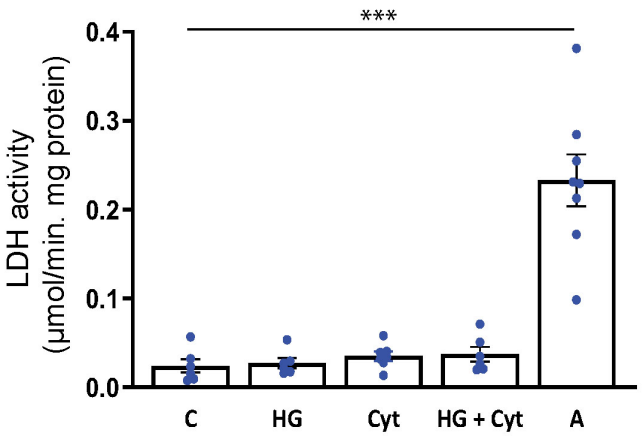

Figure 1. LDH activity in the incubation buffer. The cytotoxic effect of the short-term incubation (40 min) on the mouse retinal explants was evaluated by measuring LDH released into the incubation buffer. Although exposure to anoxic conditions resulted in statistically significantly elevated LHD release, high glucose alone and in combination with proinflammatory cytokines did not affect the LDH release compared to the control retinas. One-way analysis of variance (ANOVA) followed by post-hoc Dunnett's multiple comparison test was used to determine significance. Values represent mean ± standard error of the mean (n = 6–8 for each group). ***p<0.001. Abbreviations: A, anoxia; C, control; Cyt, proinflammatory cytokines; HG, high glucose; HG + Cyt, high glucose + proinflammatory cytokines.

Coapplication of high glucose and proinflammatory cytokines affects amino acid distribution in the retina: As statistically significant changes were observed in retinal glutamate and its release to the buffer during the incubation, we evaluated whether these changes were localized to specific cell types in the retina. For this, glutamate and related amino acids were immunolabeled (Figure 5) and further quantified (Figure 6). Figure 5A shows intensive glutamate labeling in the control retina, which spans the retinal layers except in the middle row of nuclei in the inner nuclear layer, which corresponds to the Müller cell soma. However, a statistically significant increase in glutamate immunoreactivity in the Müller cell endfeet was observed in high glucose alone (p = 0.003; Figure 5B and Figure 6A) and in combination with proinflammatory cytokines (p = 0.002; Figure 5C and Figure 6B) relative to the control retinas. In contrast, there was a statistically significant decrease in glutamate immunoreactivity in the bipolar cells (p = 0.023) of the retina coexposed to high glucose and proinflammatory cytokines relative to the control retinas. Figure 5D shows high glutamine labeling in the inner retinal layers

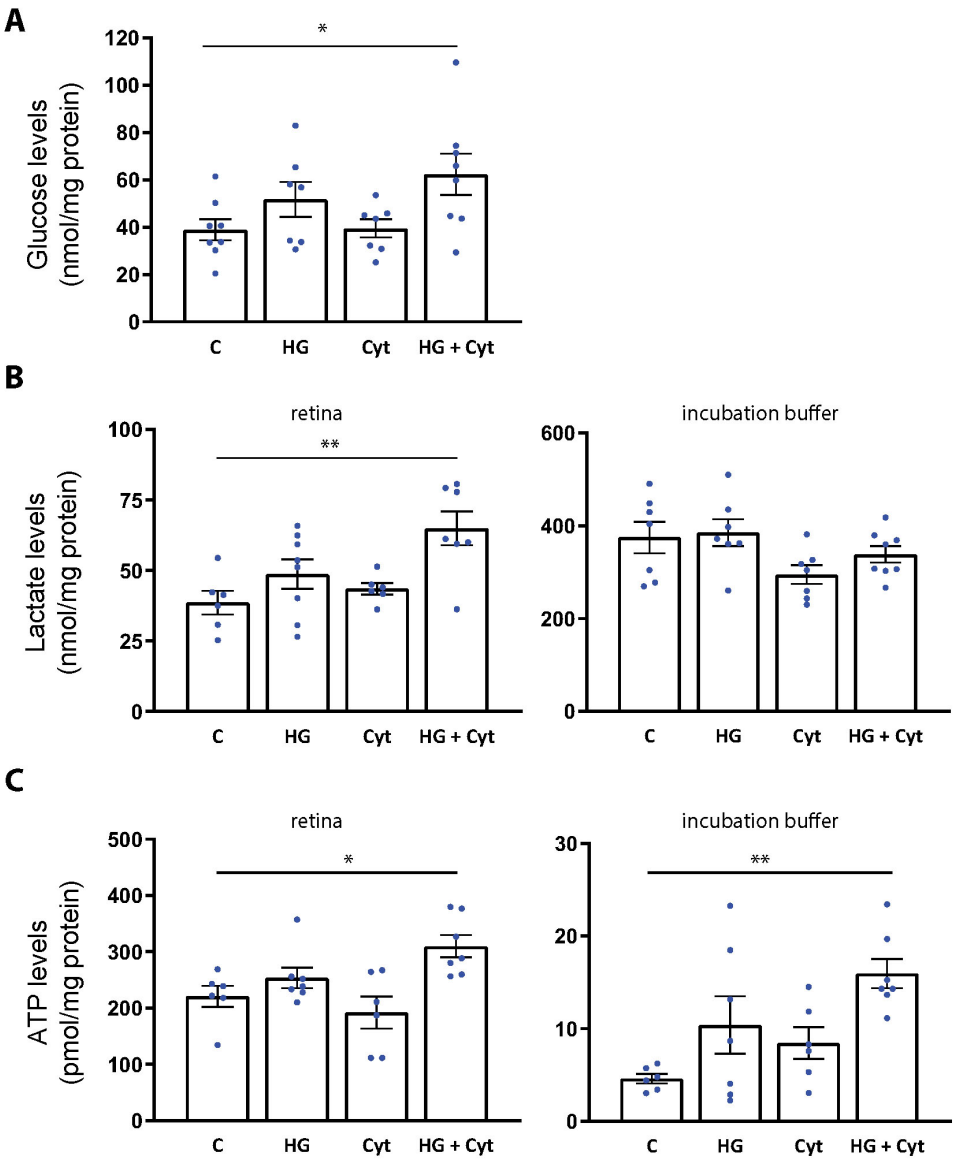

Figure 2. Key energy metabolite levels in the retina and incubation buffer. The key metabolites of retinal energy metabolism were measured in the retinal explants and incubation buffer following short-term incubation. **A**: Glucose levels in the retinal explants. **B**: Lactate levels in the retinal explants and incubation buffer. **C**: ATP levels in the retinal explants and incubation buffer. Coapplication of high glucose and proinflammatory cytokines caused a statistically significant increase in the glucose, lactate, and ATP levels, in addition to increasing ATP release relative to the control retinas. One-way analysis of variance (ANOVA) followed by post-hoc Dunnett's multiple comparison test was used to determine significance. Values represent mean ± standard error of the mean (n = 6–8 for each group). *p<0.05, **p<0.01. Abbreviations: C, control; Cyt, proinflammatory cytokines; HG, high glucose; HG + Cyt, high glucose + proinflammatory cytokines.

in the control retinas. Short-term exposure to high glucose alone did not affect glutamine immunoreactivity (Figure 5E and Figure 6C); whereas, a statistically significant decrease in glutamine labeling in Müller cell endfeet (p = 0.011) in the retinas coexposed to high glucose and proinflammatory cytokines relative to the control (Figure 5F and Figure 6D) was observed. GABA immunolabeling in the control retina (Figure 5G) showed intense reactivity in the inner plexiform layer, amacrine cells, and displaced amacrine cells, and glycine immunolabeling in the control retina showed labeling in the amacrine cells (Figure 5J). However, no statistically significant changes in GABA and glycine immunoreactivity were observed. The four individual immunogold-labeled images used in the quantification of amino acid labeling in the retinal explants are provided as Appendix 2, Appendix 3, Appendix 4 and Appendix 5.

DISCUSSION

Inflammation plays a vital role in DR progression, and evidence suggests that inflammation triggers the disease in a hyperglycemic environment [3-7]. In a recent study, intravitreal injection of proinflammatory cytokines TNF-α and IL-1β into diabetic mice with no previous ocular problems triggered the development of clinical signs of DR within 1 week [5]. Similarly, in the present study, proinflammatory cytokines and hyperglycemia triggered the loss of metabolic

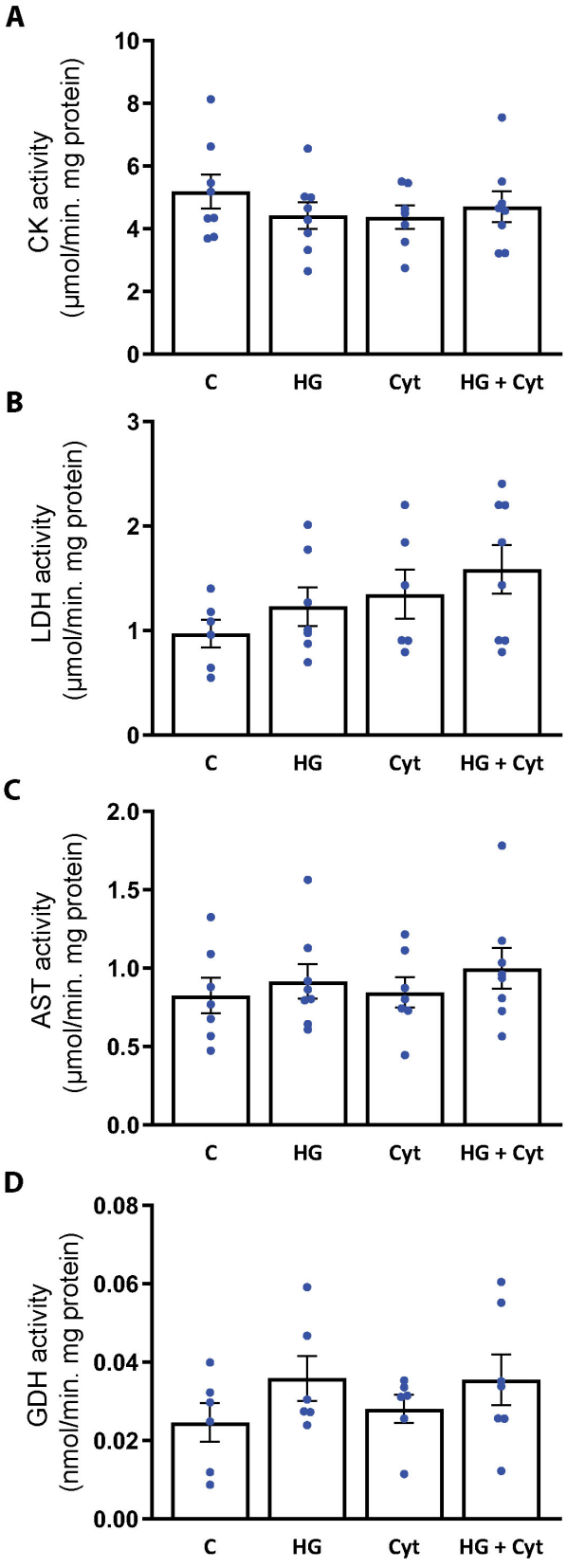

Figure 3. Activity of enzymes that support ATP levels in the retina. **A**: Creatine kinase (CK) activity. **B**: Lactate dehydrogenase (LDH) activity. **C**: Aspartate aminotransferase (AST) activity. **D**: Glutamate dehydrogenase (GDH) activity. The activities of these enzymes were unaffected under all the experimental conditions. One-way analysis of variance (ANOVA) showed no statistically significant changes (p value less than 0.05). Values represent mean ± standard error of the mean (n = 6–8 for each group). Abbreviations: C, control; Cyt, proinflammatory cytokines; HG, high glucose; HG + Cyt, high glucose + proinflammatory cytokines.

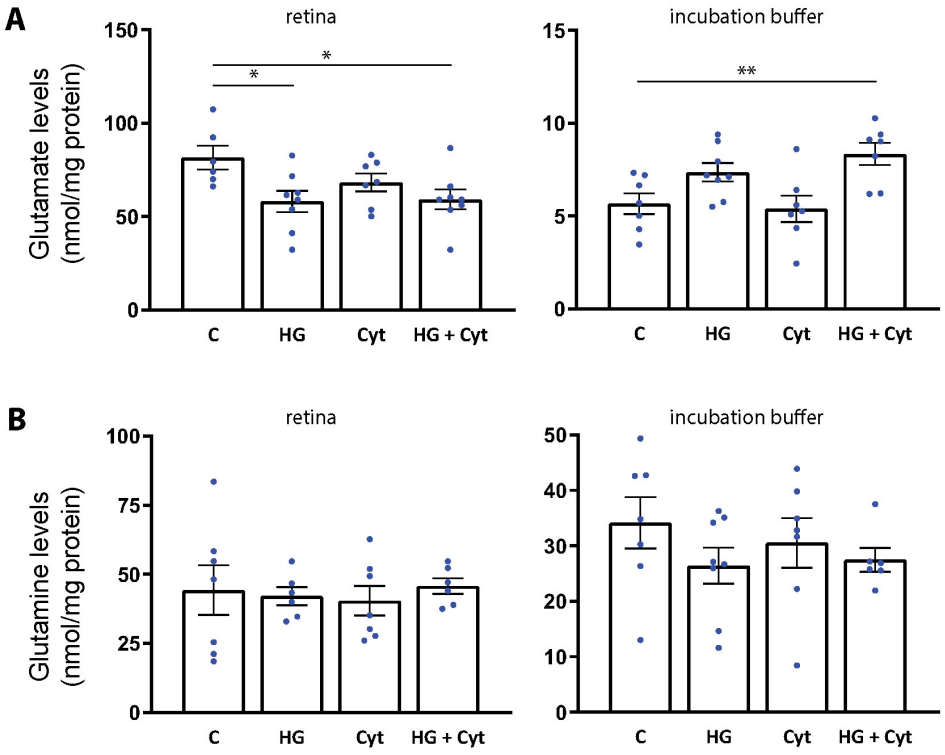

Figure 4. Glutamate and glutamine levels in retina and incubation buffer. The glutamate and glutamine levels were measured from the retinal explants and incubation buffer following short-term incubation. **A**: Glutamate levels in retinal explants and incubation buffer. **B**: The glutamate levels in the retinal explants and incubation buffer. The glutamate levels in the retinal explants exposed to high glucose alone and in combination with proinflammatory cytokines was statistically significantly reduced relative to control. The glutamate release from the retinal explants coexposed to high glucose and proinflammatory cytokines was statistically significantly elevated. One-way analysis of variance (ANOVA) followed by post-hoc Dunnett's multiple comparison test was used to determine significance. *p<0.05, **p<0.01. Values represent mean ± standard error of the mean (n = 6–8 for each group). Abbreviations: C, control; Cyt, proinflammatory cytokines; HG, high glucose; HG + Cyt, high glucose + proinflammatory cytokines.

equilibrium, shown as changes in energy metabolite levels and amino acid distribution in mouse retinal explants. We observed that the combined effect of high glucose and proinflammatory cytokines (although not cytotoxic during the short-term period of incubation) caused the retinal glucose levels to increase. Previous studies have shown that these molecules act on the retinal barrier and cause an increase in glucose uptake [32,33], which can further activate other downstream processes, including the polyol pathway, protein kinase C signaling, and advanced glycation end-products [34]. We suggest that the increase in glucose is likely to be attributed to increased uptake via the sodium-independent glucose transporter GLUT 1 [35], because GLUT 1 transporter activity is dependent on blood glucose levels [36] and cytokine exposure [37-40]. In fact, as the only transporter of glucose from blood, this early biomarker of DR is highlighted as a possible therapeutic target for prevention of DR progression [41].

Concomitantly with increased glucose levels, we found that the lactate and ATP levels were elevated, without affecting enzymes supporting ATP production in the mouse retinal explants. Although lactate production in the retina occurs constantly during periods of glycolytic stimulation [42], inflammation may induce metabolic reprogramming in activated macrophages, which can further cause an increase in glucose uptake and aerobic glycolysis (lactate production) during retinal pathology [43]. Elevated lactate levels in the retinal explants may suggest increased glucose metabolism via aerobic glycolysis to support the high energy demand during the short-term metabolic insult.

Previous findings that ATP levels in streptozotocin-induced diabetic rats remained unaltered [44] were confirmed in the present study, where the retinal explants incubated in high glucose alone did not show changes in ATP levels, until supplemented with proinflammatory cytokines. We also found that the combined application of high glucose and proinflammatory cytokines elicited statistically significant ATP release from the retinal explant, which is a known activator of the nucleotide-binding domain, leucine-rich–containing family, pyrin domain–containing-3 (NLRP3) inflammasome [45]. This intracellular inflammasome complex induces further ATP and proinflammatory cytokine release [46] which amplifies the NLRP3 inflammasome pathway in an autocrine manner in DR pathology [6]. In this scenario, proinflammatory cytokines not only regulate ATP levels but also contribute to feedback activation of the inflammasome pathway [6,47]. In addition to activating the inflammasome complex, extracellular ATP significantly

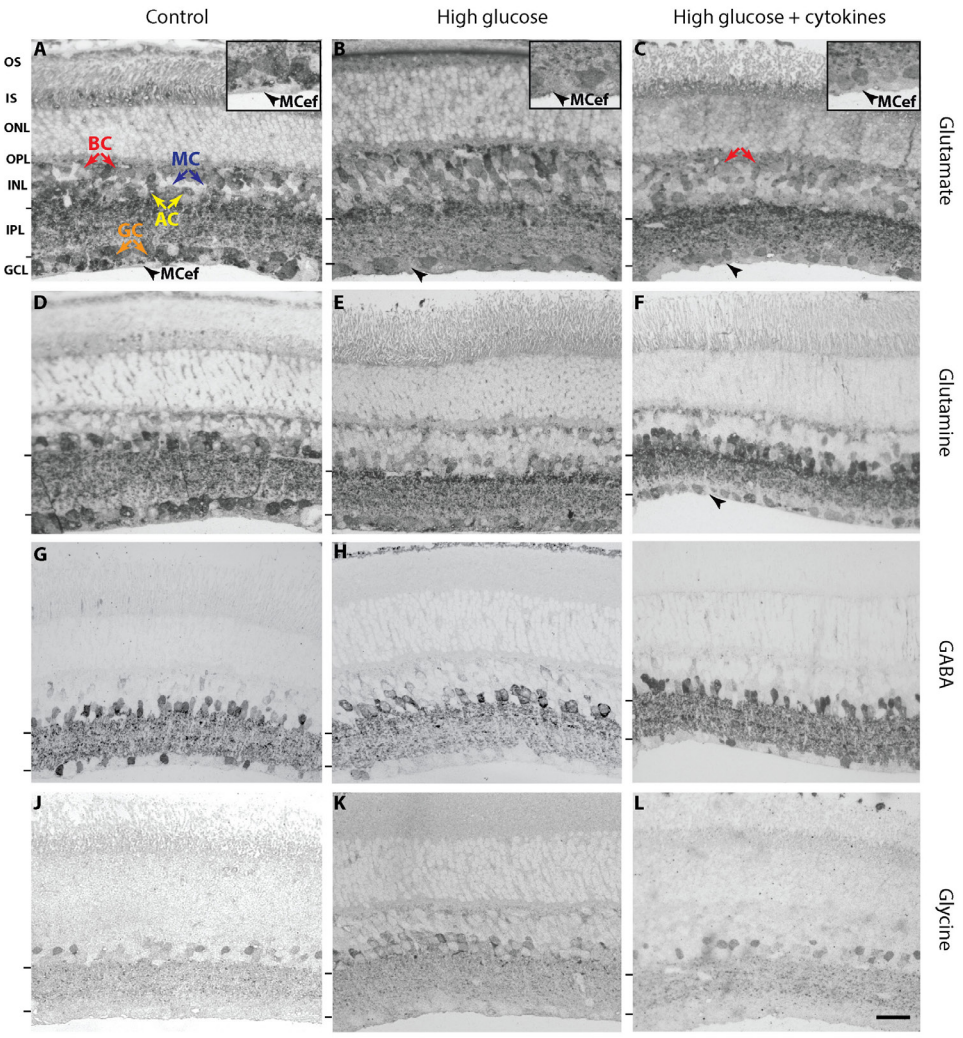

Figure 5. Representative images of immunogold labeling in retinal explants. The retinal explants (n = 4 for each group) were incubated in physiological buffer, high glucose alone and in combination with proinflammatory cytokines followed by immunolabeling for glutamate (**A**–**C**), glutamine (**D**–**F**), GABA (**G**–**I**), and glycine (**J**–**L**). The retinal layers of interest are indicated on the left side of panel **A**. The two horizontal lines on the left side of each image identify the IPL. Cells of interest are indicated in **A** with the bipolar cell, identified in the INL close to the OPL (BC, red arrow), the stellar-shape soma of Müller cells in the middle of the INL (MC, blue arrow), the amacrine cells in the lower row of the INL adjacent to the IPL (AC, yellow arrow), the cells in the ganglion cell layer (GC, orange arrow), and the intercellular space corresponding to Müller cell endfeet in the GCL (MCef, black arrowhead). **A**: Glutamate labeling in the control spans the entire retina except the middle row of nuclei in the INL, which corresponds to Müller cells. However, MCef displayed increased glutamate labeling in high glucose alone (**B**, arrowhead and insert) and in combination with proinflammatory cytokines (**C**, arrowhead and insert). Coapplication of high glucose and proinflammatory cytokines also appears to decrease glutamate labeling in bipolar cells (**C**, red arrows). D: Glutamine labeling in the control retina was seen predominantly in the inner retinal layers. A decrease in glutamine distribution was apparent in the MCef in the high glucose and proinflammatory cytokine condition (**F**, arrowhead) but not in high glucose alone (**E**). GABA labeling in the control retina was evident in amacrine cells, IPL, and displaced amacrine cells in the GCL (**G**), with no apparent differences in high glucose alone (**H**) or in combination with proinflammatory cytokines (**I**). Glycine immunolabeling was seen in amacrine cells in the control retina (**J**) with no apparent differences in high glucose alone (**K**) or in combination with proinflammatory cytokines (**L**). Scale bar is equal to 25 µm. Abbreviations: AC, amacrine cell; BC, bipolar cell; GC, ganglion cell; GCL, ganglion cell layer; INL, inner nuclear layer; IPL, inner plexiform layer; IS, photoreceptor inner segment; MC, Müller cell; MCef, Müller cell endfeet; ONL, outer nuclear layer; OPL, outer plexiform layer; OS, photoreceptor outer segment.

contributes to adenosinergic and purinergic signaling in DR conditions [48,49], two of the other well-known regulators of inflammasome activity [46]. In addition to ATP, a recent study reported that glutamate activated N-methyl-D-aspartate (NMDA)-mediated excitotoxicity induced NLRP3 inflammasome activity [50]. Correspondingly, in the present study, we observed increased glutamate release from the retinal explants coexposed to high glucose and proinflammatory cytokines. Moreover, increased glutamate accumulation in Müller cell endfeet under these conditions can hinder and slow the glutamate clearance from the synaptic cleft by affecting glutamate uptake [51]. Taken together, these conditions may promote glutamate-mediated excitotoxicity and may act as activators of the NLRP3 inflammasome complex. Glutamate accumulation within the Müller cell endfeet may be attributed to downregulation or inactivation of the

critical glutamate metabolizing enzyme, glutamine synthetase [52]. IL-1β was found to significantly decrease glutamine synthetase expression in Müller cells under high glucose conditions [53], and in support, we observed a localized

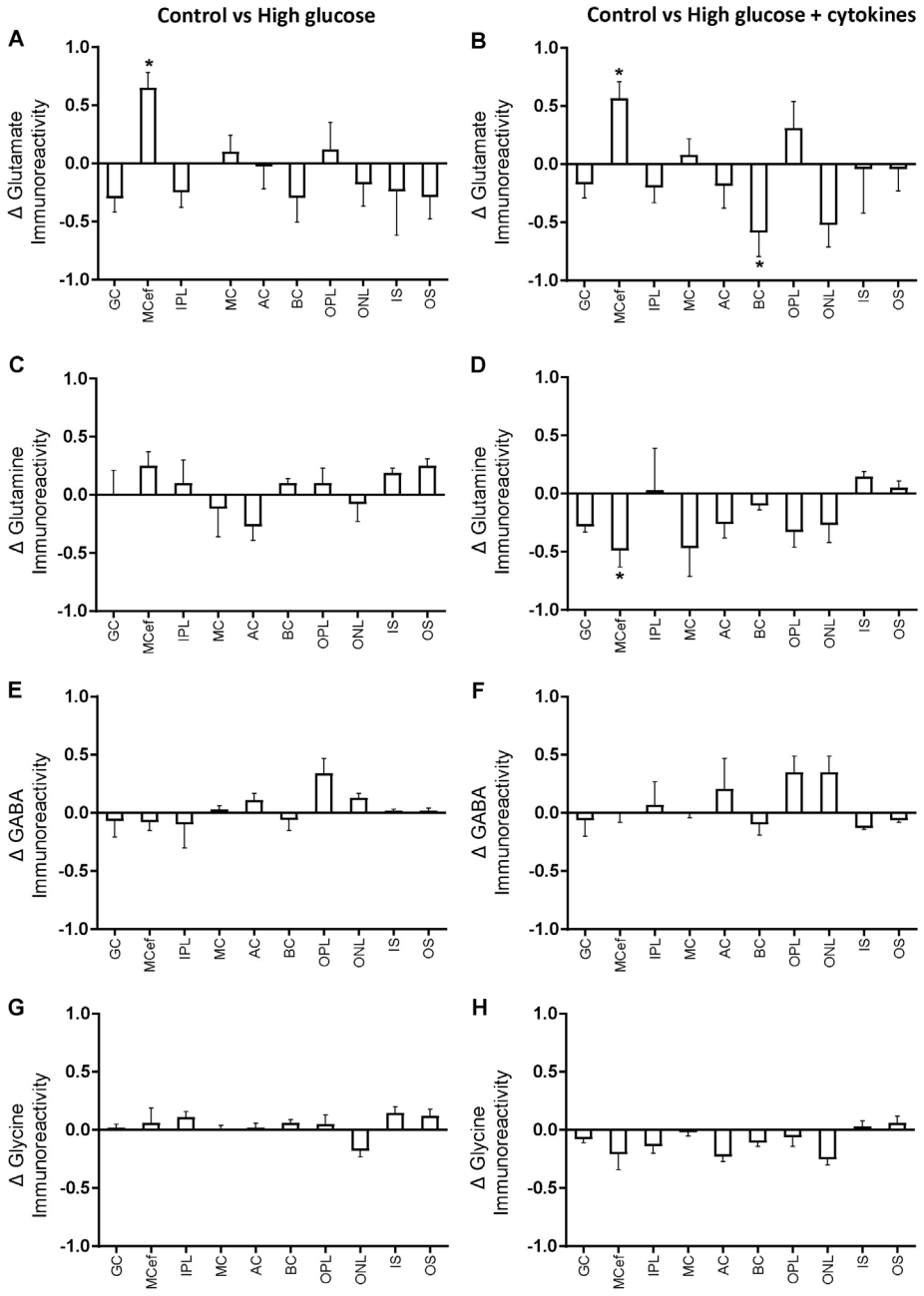

Figure 6. Quantification of the relative changes in amino acid labeling. **A**, **B**: Glutamate. **C**, **D**: Glutamine. **E**, **F**: GABA. **G**, **H**: Glycine; (n = 4 for each group). **A**, **C**, **E**, **G** represent the relative changes in amino acid labeling in high glucose alone compared to control, whereas **B**, **D**, **F**, and **H** show the relative change in in amino acid labeling in the high glucose and proinflammatory cytokines condition compared to the control retinas. Each value represents the mean difference in immunoreactivity relative to the control condition and is presented as mean percentage change ± standard error of the mean. One-way analysis of variance (ANOVA) followed by post-hoc Dunnett's multiple comparison test was used to determine significance. *p<0.05. Abbreviations: AC, amacrine cell; BC, bipolar cell; GCL, ganglion cell layer; IPL, inner plexiform layer; IS, photoreceptor inner segments; MC, Müller cell; MCef, Müller cell endfeet; ONL, outer nuclear layer; OPL, outer plexiform layer; OS, photoreceptor outer segments.

decrease in glutamine levels in Müller cell endfeet. Moreover, these proinflammatory cytokines were found to affect the capacity of Müller cells to uptake glutamate and cause glutamate excitotoxicity [54]. Despite the elevated retinal ATP levels, there were no changes in the AST and GDH activities, implying that glutamate was not metabolized via the TCA cycle to support the high energy demand. However, we reason that the reduced glutamate levels in high glucose alone and in combination with proinflammatory cytokines were due to a rapid decrease in glutamate synthesis (within 15 min) from carbon dioxide rather than from glutamine [25]. Similarly, in the present study, the glutamine levels were unchanged under these conditions. Interestingly, in addition to proinflammatory cytokines, lactate accumulation was found to impede glutamate uptake and promote extracellular glutamate release [55]. Localized changes in glutamate and glutamine levels in the cells of the inner retina imply that the metabolic insult affects the inner retina more than the outer retina, which is in agreement with clinical signs that show the inner retinal layers are affected more than the outer retinal layers in patients with DR [56].

In conclusion, the present study results support the hypothesis that proinflammatory cytokines accelerate the retinal biochemical and neurochemical changes that occur in a hyperglycemic microenvironment. Furthermore, short-term exposure of the retina to high glucose and proinflammatory cytokines alters the key metabolites of energy metabolism and causes amino acid redistribution affecting the bipolar and Müller cells in the inner retina. Moreover, inflammasome assembly may be occurring early in the DR condition. The prospect of patients with diabetes being at risk of DR development in a retinal inflammatory environment highlights the need to evaluate early therapeutic strategies to provide good metabolic control and prevent DR progression.

APPENDIX 1. KEY METABOLITE LEVELS AND ENZYME ACTIVITIES OF RETINAL EXPLANTS INCUBATED IN D-MANNITOL.

To access the data, click or select the words "Appendix 1." Incubation of retinal explants in D-mannitol did not significantly alter key metabolite levels and enzyme activities. A: Glucose levels ($p = 0.588$). B: Lactate levels ($p = 0.220$). C: ATP levels ($p = 0.051$). D: Glutamate levels ($p = 0.877$). E: Glutamine levels ($p = 0.274$). F: CK activity ($p = 0.436$). G: LDH activity ($p = 0.871$). H: AST activity ($p = 0.543$). I: GDH activity ($p = 0.713$). Student's t-test was used to determine statistical significance. Values represent mean ± standard error of the mean. Abbreviations: C-control, M- D-mannitol.

APPENDIX 2. THE FOUR IMMUNOGOLD LABELED IMAGES USED TO QUANTIFY GLUTAMATE LABELING IN RETINAL EXPLANTS.

To access the data, click or select the words "Appendix 2." Glutamate labeling in control (A-D), high glucose alone (E-H) and high glucose in combination with proinflammatory cytokines (I-L) condition. The retinal layers of interest are indicated on the left-hand side of image A. The two horizontal lines on the left-hand side of each image identify the IPL. Cells of interest are indicated in image A with the bipolar cell, identified in the INL close to the OPL (BC-red arrow), the stellar-shape soma of Müller cells in the middle of the INL (MC-blue arrow), the amacrine cells in the lower row of the INL adjacent to the IPL (AC-yellow arrow), the cells in the ganglion cell layer (GC-orange arrow), and the intercellular space corresponding to Müller cell endfeet in the GCL (MCef- black arrowhead). Glutamate labeling in MCef (arrowhead and insert) displayed increased labeling in high glucose alone (E-H), and in combination with proinflammatory cytokines (I-L). Coapplication of high glucose and proinflammatory cytokines also displayed decreased glutamate labeling in bipolar cells (red arrows in I-H). Scale bar is equal to 25 µm. Abbreviations: OS-photoreceptor outer segment; IS-photoreceptor inner segment; ONL-outer nuclear layer; OPL-outer plexiform layer; INL- inner nuclear layer; IPL-inner plexiform layer; GCL-ganglion cell layer.

APPENDIX 3. THE FOUR IMMUNOGOLD LABELED IMAGES USED TO QUANTIFY GLUTAMINE LABELING IN RETINAL EXPLANTS.

To access the data, click or select the words "Appendix 3." Glutamine labeling in control (A-D), high glucose alone (E-H) and high glucose in combination with proinflammatory cytokines (I-L) condition. The retinal layers of interest are indicated on the left-hand side of image A. The two horizontal lines on the left-hand side of each image identify the IPL. Glutamine labeling in MCef displayed decreased labeling in high glucose in combination with proinflammatory cytokines (I-L) condition. Scale bar is equal to 25 µm. Abbreviations: OS-photoreceptor outer segment; IS-photoreceptor inner segment; ONL-outer nuclear layer; OPL-outer plexiform layer; INL- inner nuclear layer; IPL-inner plexiform layer; GCL-ganglion cell layer.

APPENDIX 4. THE FOUR IMMUNOGOLD LABELED IMAGES USED TO QUANTIFY GABA LABELING IN RETINAL EXPLANTS.

To access the data, click or select the words "Appendix 4." GABA labeling in control (A-D), high glucose alone (E-H) and high glucose in combination with proinflammatory cytokines (I-L) condition. The retinal layers of interest are indicated on the left-hand side of image A. The two horizontal lines on the left-hand side of each image identify the IPL. Scale bar is equal to 25 µm. Abbreviations: OS-photoreceptor outer segment; IS-photoreceptor inner segment; ONL-outer nuclear layer; OPL-outer plexiform layer; INL- inner nuclear layer; IPL-inner plexiform layer; GCL-ganglion cell layer.

APPENDIX 5. THE FOUR IMMUNOGOLD LABELED IMAGES USED TO QUANTIFY GLYCINE LABELING IN RETINAL EXPLANTS.

To access the data, click or select the words "Appendix 5." Glycine labeling in control (A-D), high glucose alone (E-H) and high glucose in combination with proinflammatory cytokines (I-L) condition. The retinal layers of interest are indicated on the left-hand side of image A. The two horizontal lines on the left-hand side of each image identify the IPL. Scale bar is equal to 25 µm. Abbreviations: OS-photoreceptor outer segment; IS-photoreceptor inner segment; ONL-outer nuclear layer; OPL-outer plexiform layer; INL- inner nuclear layer; IPL-inner plexiform layer; GCL-ganglion cell layer.

ACKNOWLEDGMENTS

Gaganashree Shivashankar is currently supported by the Dean's International Doctoral Scholarship from the Faculty of Medical and Health Sciences, University of Auckland, New Zealand. This study was partially funded by Maurice and Phyllis Paykel Trust grant (3715457) and The New Zealand Optometric Vision Research Foundation grant (3717092). The authors would like to thank Dr. Arier Lee for her support with the statistical analysis. The authors declare no conflict of interest.

REFERENCES

1. Durham JT, Herman IM. Microvascular modifications in diabetic retinopathy. Curr Diab Rep 2011; 11:253-64. [PMID: 21611764].
2. Antonetti DA, Barber AJ, Bronson SK, Freeman WM, Gardner TW, Jefferson LS, Kester M, Kimball SR, Krady JK, LaNoue KF, Norbury CC, Quinn PG, Sandirasegarane L, Simpson IA. JDRF Diabetic Retinopathy Center GroupDiabetic retinopathy: Seeing beyond glucose-induced microvascular disease. Diabetes 2006; 55:2401-11. [PMID: 16936187].
3. Adamis AP. Is diabetic retinopathy an inflammatory disease? Br J Ophthalmol 2002; 86:363-5. [PMID: 11914197].
4. Kern TS. Contributions of inflammatory processes to the development of the early stages of diabetic retinopathy. Exp Diabetes Res 2007; 2007:95103-14. [PMID: 18274606].
5. Mugisho OO, Rupenthal ID, Squirrell DM, Bould SJ, Danesh-Meyer HV, Zhang J, Green CR, Acosta ML. Intravitreal pro-inflammatory cytokines in non-obese diabetic mice: Modelling signs of diabetic retinopathy. PLoS One 2018; 13:e0202156-[PMID: 30133488].
6. Mugisho OO, Green CR, Kho DT, Zhang J, Graham ES, Acosta ML, Rupenthal ID. The inflammasome pathway is amplified and perpetuated in an autocrine manner through connexin43 hemichannel mediated ATP release. Biochim Biophys Acta, Gen Subj 2018; 1862:385-93. [PMID: 29158134].
7. Mugisho OO, Green CR, Zhang J, Binz N, Acosta ML, Rakoczy E, Rupenthal ID. Immunohistochemical characterization of Connexin43 expression in a mouse model of diabetic retinopathy and in human donor retinas. Int J Mol Sci 2017; 18:2567-[PMID: 29186067].
8. Sohn EH, van Dijk HW, Jiao C, Kok PH, Jeong W, Demirkaya N, Garmager A, Wit F, Kucukevcilioglu M, vanVelthoven ME, DeVries JH, Mullins RF, Kuehn MH, Schlingemann RO, Sonka M, Verbraak FD, Abràmoff MD. Retinal neurodegeneration may precede microvascular changes characteristic of diabetic retinopathy in diabetes mellitus. Proc Natl Acad Sci USA 2016; 113:E2655-64. [PMID: 27114552].
9. Ames A, Li YY, Heher EC, Kimble CR. Energy metabolism of rabbit retina as related to function: High cost of Na+ transport. J Neurosci 1992; 12:840-53. [PMID: 1312136].
10. Wang L, Törnquist P, Bill A. Glucose metabolism of the inner retina in pigs in darkness and light. Acta Physiol Scand 1997; 160:71-4. [PMID: 9179313].
11. Rogatzki MJ, Ferguson BS, Goodwin ML, Gladden LB. Lactate is always the end product of glycolysis. Front Neurosci 2015; 9:22-[PMID: 25774123].
12. Kennedy BG, Haley BE, Mangini NJ. Creatine kinase in human retinal pigment epithelium. Exp Eye Res 2000; 70:183-90. [PMID: 10655143].
13. Acosta ML, Fletcher EL, Azizoglu S, Foster LE, Farber DB, Kalloniatis M. Early markers of retinal degeneration in rd/rd mice. Mol Vis 2005; 11:717-28. [PMID: 16163270].
14. Acosta ML, Kalloniatis M. Short- and long-term enzymatic regulation secondary to metabolic insult in the rat retina. J Neurochem 2005; 92:1350-62. [PMID: 15748154].
15. Acosta ML, Shin YS, Ready S, Fletcher EL, Christie DL, Kalloniatis M. Retinal metabolic state of the proline-23-histidine rat model of retinitis pigmentosa. Am J Physiol Cell Physiol 2010; 298:764-74. [PMID: 20032515].
16. Erecińska M, Silver IA. Metabolism and role of glutamate in mammalian brain. Prog Neurobiol 1990; 35:245-96. [PMID: 1980745].

17. Bui BV, Hu RG, Acosta ML, Donaldson P, Vingrys AJ, Kalloniatis M. Glutamate metabolic pathways and retinal function. J Neurochem 2009; 111:589-99. [PMID: 19702659].

18. Kalloniatis M, Loh CS, Acosta ML, Tomisich G, Zhu Y, Nivison-Smith L, Fletcher EL, Chua J, Sun D, Arunthavasothy N. Retinal amino acid neurochemistry in health and disease. Clin Exp Optom 2013; 96:310-32. [PMID: 23464379].

19. Santiago AR, Gaspar JM, Baptista FI, Cristovao AJ, Santos PF, Kamphuis W, Ambrosio AF. Diabetes changes the levels of ionotropic glutamate receptors in the rat retina. Mol Vis 2009; 15:1620-30. [PMID: 19693289].

20. Bringmann A, Grosche A, Pannicke T, Reichenbach A. GABA and glutamate uptake and metabolism in retinal glial (Müller) cells. Front Endocrinol 2013; 4:48-[PMID: 23616782].

21. Schousboe A, Bak LK, Waagepetersen HS. Astrocytic control of biosynthesis and turnover of the neurotransmitters glutamate and GABA. Front Endocrinol (Lausanne) 2013; 4:102-[PMID: 23966981].

22. Magistretti PJ, Pellerin L. Cellular mechanisms of brain energy metabolism and their relevance to functional brain imaging. Philos Trans R Soc Lond B Biol Sci 1999; 354:1155-63. [PMID: 10466143].

23. Marani E, Ruigrok TJ. Enzyme histochemical changes in retinal ganglion cells and the optic nerve after goldfish optic nerve lesion. A regenerative and hypertrophic phenomena study. Acta Morphol Neerl Scand 1984; 22:97-114. [PMID: 6485896].

24. Pulido JE, Pulido JS, Erie JC, Arroyo J, Bertram K, Lu MJ, Shippy SA. A role for excitatory amino acids in diabetic eye disease. Exp Diabetes Res 2007; 2007:36150-7. [PMID: 17713594].

25. Gowda K, Zinnanti WJ, LaNoue KF. The influence of diabetes on glutamate metabolism in retinas. J Neurochem 2011; 117:309-20. [PMID: 21288239].

26. Nivison-Smith L, Acosta ML, Misra S, O'Brien BJ, Kalloniatis M. Vinpocetine regulates cation channel permeability of inner retinal neurons in the ischaemic retina. Neurochem Int 2014; 66:1-14. [PMID: 24412512].

27. Edwards FA, Konnerth A, Sakmann B, Takahashi T. A thin slice preparation for patch clamp recordings from neurones of the mammalian central nervous system. Pflugers Arch 1989; 414:600-12. [PMID: 2780225].

28. Strug I, Utzat C, Cappione A, Gutierrez S, Amara R, Lento J, Capito F, Skudas R, Chernokalskaya E, Nadler T. Development of a univariate membrane-based mid-infrared method for protein quantitation and total lipid content analysis of biological samples. J Anal Methods Chem 2014; 2014:657079-12. [PMID: 25371845].

29. Debnam PM, Shearer G. Colorimetric assay for substrates of NADP+-dependent dehydrogenases based on reduction of a tetrazolium dye to its soluble formazan. Anal Biochem 1997; 250:253-5. [PMID: 9245447].

30. Kalloniatis M, Fletcher EL. Immunocytochemical localization of the amino acid neurotransmitters in the chicken retina. J Comp Neurol 1993; 336:174-93. [PMID: 7902364].

31. Marc RE, Liu WL, Kalloniatis M, Raiguel SF, van Haesendonck E. Patterns of glutamate immunoreactivity in the goldfish retina. J Neurosci 1990; 10:4006-34. [PMID: 1980136].

32. Busik JV, Mohr S, Grant MB. Hyperglycemia-induced reactive oxygen species toxicity to endothelial cells is dependent on paracrine mediators. Diabetes 2008; 57:1952-65. [PMID: 18420487].

33. Busik JV, Olson LK, Grant MB, Henry DN. Glucose-induced activation of glucose uptake in cells from the inner and outer blood-retinal barrier. Invest Ophthalmol Vis Sci 2002; 43:2356-63. [PMID: 12091438].

34. Sears N, Yuan A. A basic scientific understanding of diabetic retinopathy. In: Singh RP, editor. Managing Diabetic Eye Disease in Clinical Practice. Switzerland: Springer International Publishing; 2015. p. 13–24.

35. Kumagai AK. Glucose transport in brain and retina: Implications in the management and complications of diabetes. Diabetes Metab Res Rev 1999; 15:261-73. [PMID: 10495475].

36. Cloherty EK, Diamond DL, Heard KS, Carruthers A. Regulation of GLUT1-mediated sugar transport by an antiport/uniport switch mechanism. Biochemistry 1996; 35:13231-9. [PMID: 8855962].

37. Wieman HL, Wofford JA, Rathmell JC. Cytokine stimulation promotes glucose uptake via phosphatidylinositol-3 kinase/Akt regulation of Glut1 activity and trafficking. Mol Biol Cell 2007; 18:1437-46. [PMID: 17301289].

38. Pekala P, Marlow M, Heuvelman D, Connolly D. Regulation of hexose transport in aortic endothelial cells by vascular permeability factor and tumor necrosis factor-alpha, but not by insulin. J Biol Chem 1990; 265:18051-[PMID: 2211680].

39. Boado RJ, Pardridge WM. Measurement of blood-brain barrier GLUT1 glucose transporter and actin mRNA by a quantitative polymerase chain reaction assay. J Neurochem 1994; 62:2085-90. [PMID: 8189217].

40. Vaughan RA, Garcia-Smith R, Dorsey J, Griffith JK, Bisoffi M, Trujillo KA. Tumor necrosis factor alpha induces Warburg-like metabolism and is reversed by anti-inflammatory curcumin in breast epithelial cells. Int J Cancer 2013; 133:2504-10. [PMID: 23661584].

41. Lu L, Seidel CP, Iwase T, Stevens RK, Gong YY, Wang X, Hackett SF, Campochiaro PA. Suppression of GLUT1; A new strategy to prevent diabetic complications. J Cell Physiol 2013; 228:251-7. [PMID: 22717959].

42. Winkler BS. Retinal aerobic glycolysis revisited. Invest Ophthalmol Vis Sci 1989; 30:1023-[PMID: 2732017].

43. Léveillard T, Philp NJ, Sennlaub F. Is retinal metabolic dysfunction at the center of the pathogenesis of age-related macular degeneration? Int J Mol Sci 2019; 20:E762-[PMID: 30754662].

44. Osorio-Paz I, Uribe-Carvajal S, Salceda R. In the early stages of diabetes, rat retinal mitochondria undergo mild uncoupling

due to UCP2 activity. PLoS One 2015; 10:e0122727-[PMID: 25951172].

45. Kim Y, Davidson JO, Gunn KC, Phillips AR, Green CR, Gunn AJ. Role of hemichannels in CNS inflammation and the inflammasome pathway. Adv Protein Chem Struct Biol 2016; 104:1-37. [PMID: 27038371].

46. Gombault A, Baron L, Couillin I. ATP release and purinergic signaling in NLRP3 inflammasome activation. Front Immunol 2013; 3:414-[PMID: 23316199].

47. Elliott EI, Sutterwala FS. Initiation and perpetuation of NLRP3 inflammasome activation and assembly. Immunol Rev 2015; 265:35-52. [PMID: 25879282].

48. Vindeirinho J, Santiago AR, Cavadas C, Ambrósio AF, Santos PF. The adenosinergic system in diabetic retinopathy. J Diabetes Res 2016; 2016:4270301-8. [PMID: 27034960].

49. Reichenbach A, Bringmann A. Purinergic signaling in retinal degeneration and regeneration. Neuropharmacology 2016; 104:194-211. [PMID: 25998275].

50. Tsoka P, Barbisan PR, Kataoka K, Chen XN, Tian B, Bouzika P, Miller JW, Paschalis EI, Vavvas DG. NLRP3 inflammasome in NMDA-induced retinal excitotoxicity. Exp Eye Res 2019; 181:136-44. [PMID: 30707890].

51. Li Q, Puro DG. Diabetes-induced dysfunction of the glutamate transporter in retinal Müller cells. Invest Ophthalmol Vis Sci 2002; 43:3109-16. [PMID: 12202536].

52. Lieth E, LaNoue KF, Antonetti DA, Ratz M. Diabetes reduces glutamate oxidation and glutamine synthesis in the retina. The Penn State Retina Research Group. Exp Eye Res 2000; 70:723-30. [PMID: 10843776].

53. Shen X, Xu G. Role of IL-1beta on the glutamine synthetase in retinal Müller cells under high glucose conditions. Curr Eye Res 2009; 34:727-36. [PMID: 19839866].

54. Zou JY, Crews FT. TNFα potentiates glutamate neurotoxicity by inhibiting glutamate uptake in organotypic brain slice cultures: Neuroprotection by NFκB inhibition. Brain Res 2005; 1034:11-24. [PMID: 15713255].

55. Bender AS, Young LP, Norenberg MD. Effect of lactic acid on L-glutamate uptake in cultured astrocytes: Mechanistic considerations. Brain Res 1997; 750:59-66. [PMID: 9098530].

56. Vujosevic S, Midena E. Retinal layers changes in human preclinical and early clinical diabetic retinopathy support early retinal neuronal and Müller cells alterations. J Diabetes Res 2013; 2013:905058-8. [PMID: 23841106].

Articles are provided courtesy of Emory University and the Zhongshan Ophthalmic Center, Sun Yat-sen University, P.R. China. The print version of this article was created on 11 April 2020. This reflects all typographical corrections and errata to the article through that date. Details of any changes may be found in the online version of the article.